THE TESTING AND CHARACTERIZATION OF THE CHEOPS CCDS

A. Deline[1], M. Sordet[1], F. Wildi[1], B. Chazelas[1].

[1]University of Geneva, Astronomy dpt., 51 ch. des Maillettes, CH-1290 Sauverny, Switzerland.

I. INTRODUCTION:

The Characterising Exoplanet Satellite (CHEOPS) (Fig. 1) is a European Space Agency (ESA) mission dedicated to search for transits by means of ultra-high-precision photometry on bright stars already known to host planets [1,2]. One of the most challenging requirements is to reach a 20ppm photometric accuracy over 6 hours, which should allow CHEOPS to detect super-earths transiting very bright stars. The launch is scheduled at the beginning of 2018 and will place the satellite on a Sun-Synchronous Orbit (SSO) at about 700 km.

Fig. 1. (*Left*) CHEOPS. (*Right*) Back-illuminated CCD sensor

CHEOPS' only instrument is a 320mm-diameter Ritchey-Chrétien telescope producing slightly defocused images. At the focal plane of the instrument is a back-illuminated charge-coupled device (CCD) (Fig. 1) thermally stabilised at -40°C covering the wavelength range 400-1100 nm. In the rest of this article, we use the acronym CHEOPS to refer to the CHEOPS instrument.

In order to reach the required photometric precision, CHEOPS will be calibrated before launch on a specifically developed on-ground calibration bench [3,4].

Prior to that phase, the characterisation of the detector was necessary. ESA provided three flight models (FM) to be characterised and then compared to each other in order to select the best one for the satellite. A CCD test bench was designed and manufactured to measure the performances of these sensors.

This article presents the test principles and the results of the CCD selected to be integrated in the satellite. All three FM have been characterized but because of the duration required, only the selected FM has been submitted to a fine grained characterisation of the gain to all bias voltages combinations.

II. TEST SET-UP DESIGN:

The characterisation of the CCDs has been performed with a test bench specifically designed to provide the following required measurements:

- the bias level and read-out noise (RON)
- the dark current
- the system gain
- the non-linearity
- the Photo-Response Non-Uniformity (PRNU)
- the Quantum Efficiency (QE)

As no point source was needed for these measurements, the test set-up only provided a uniform illumination of the CCD with a highly stable light source. Fig. 2 represents a diagram of the CCD characterization system, which is described below.
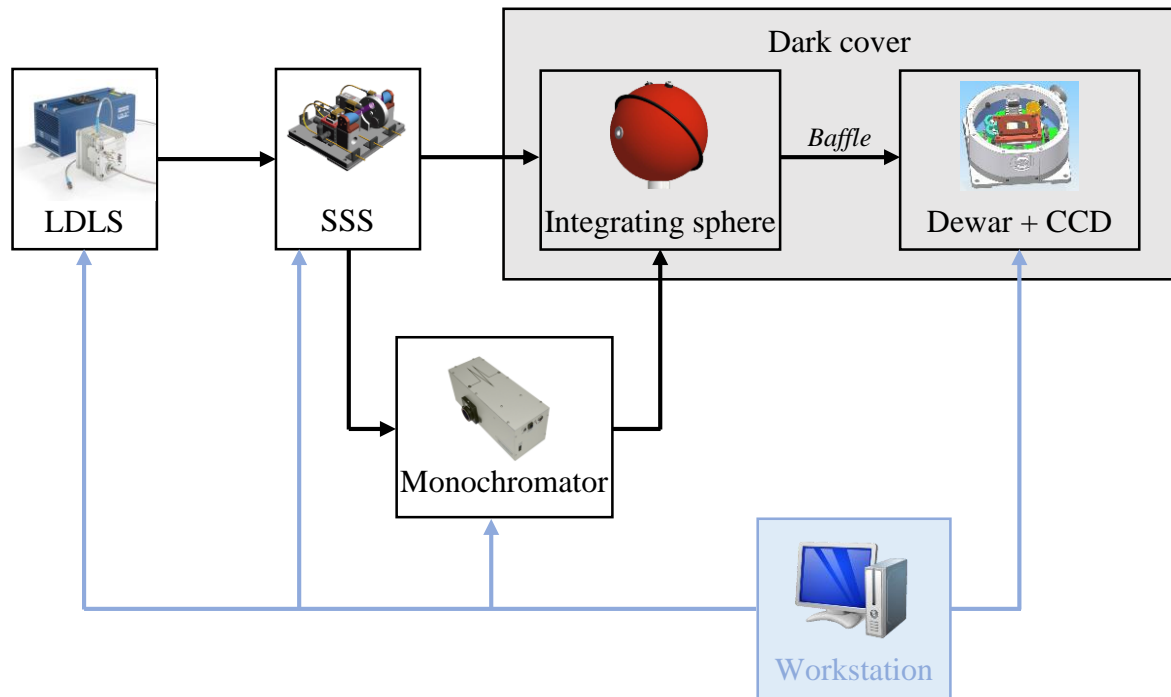
Fig. 2. Diagram of the CCD characterization system

A. Optical chain

   The primary source of the optical chain is a Laser-Driven Light Source (LDLS) from Energetiq [5] that produces a 10'000K colour temperature over a flat spectrum covering our wavelength range of interest. The intensity variation of the LDLS has an amplitude of about 2% over 6 hours, which is much higher than the specified CHEOPS performance of 20 ppm.

   Therefore, this source was coupled with a stabilizing system called Super Stable Source (SSS) [6], developed and patented by the University of Geneva. The SSS reduces the source variations down to a few ppm rms when the signal is averaged in 1-min bins (Fig. 3), and injects the stabilised beam into a large multimode fibre.
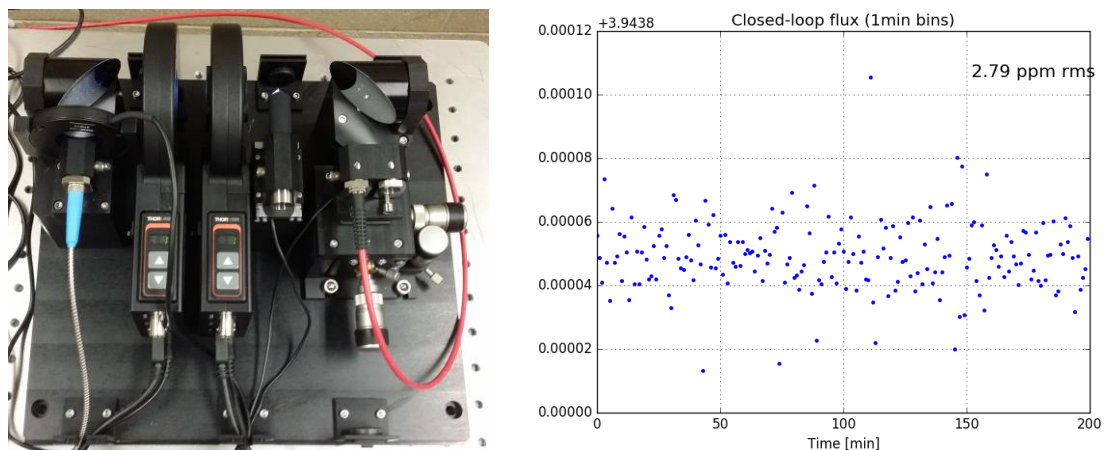

Fig. 3. (*Left*) Picture of the SSS system. (*Right*) Flux stabilised with the SSS.

   The uniform illumination of the CCD is ensured by a high-quality integrating sphere. Its large $\emptyset_{sphere}$-to-$\emptyset_{port}$ ratio has been chosen to guarantee a good flatness over the whole CCD. A baffle has also been designed and integrated between the sphere and the CCD to avoid reflected light contamination and increase uniformity.

   As PRNU and QE measurements require monochromatic images, the test bench allows to integrate a monochromator between the SSS and the integrating sphere. This device allows the selection 16nm-large wavelength bands every 50nm across CHEOPS spectral range.

B. CCD cryostat

The CCD characterisation was performed at operating temperature. Therefore, a full featured cryostat was designed around the sensor (Fig. 4) including a vacuum enclosure, a temperature control, signal conditioning board and an optical interface (window). The temperature of the CCD was maintained at -40°C with a mK precision and an ambient pressure of about 10^{-6} mbar.
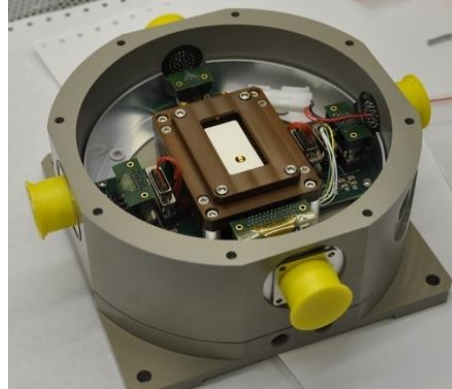

Fig. 4. The CCD test cryostat designed and assembled by the University of Geneva.

III. TEST RESUTS:

The different tests have all been performed on the three flight model (FM) CCDs in order to select the best one to be integrated in CHEOPS spacecraft.

The following sections describe the test procedures and show the results for the selected CCD.

A. Bias level and Read-out noise

The bias level is measured by making zero-integration time exposures with the CCD in the dark. The standard deviation of the bias image is called the read-out noise.

The bias level was computed for each pixel by calculating their average value. A high-quality bias map was generated thanks to the combination of 1'000 images allowing to reduce the noise contribution by a factor of about 30 (Fig. 5). This map was then used to remove the bias contribution in subsequent measurements.

The RON was estimated as the average value of the standard deviations of all the images (Fig. 5), leading to a value of 4.027 ADU. The detector RON can be obtained by quadratically removing the electronic noise. Expressed in electrons using the gain calculated in subsection C, one gets a RON of 5.35 e⁻.
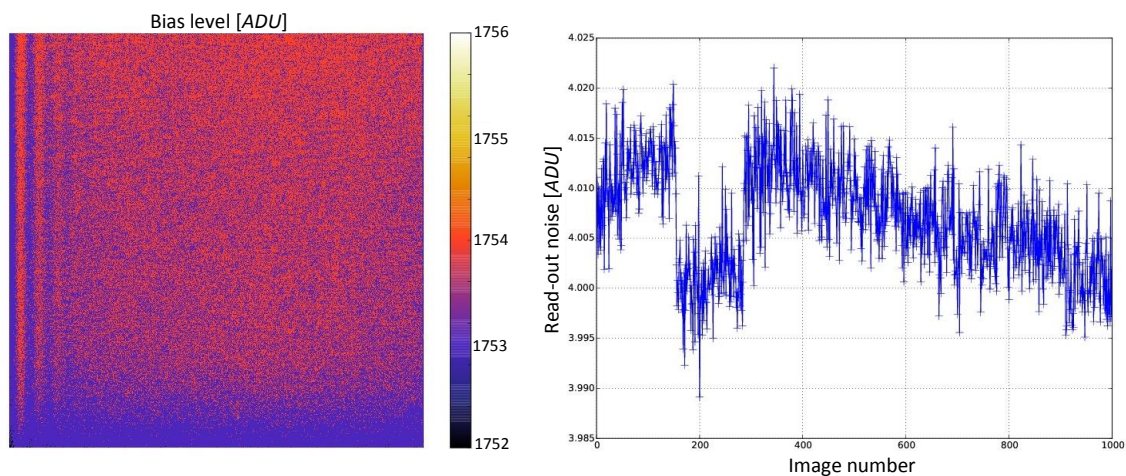

Fig. 5. (*Left*) Bias image of the CCD with an average value of 1753.5 ADU.
(*Right*) Read-out noise of 1'000 successive images (noise computed over the whole frame).

B. Dark current

The dark signal is measured by making exposures with the CCD placed in the dark at different temperatures. Two kinds of performances are extracted from this data set: the average dark current versus CCD temperature and the dark current in each pixel at -40°C (nominal temperature). The dark current is calculated on the whole image by subtracting the bias level and dividing the residual signal by the exposure time in order to get the dark current in ADU/s.

From the dark current map, we identify the hot and warm pixels and the standard deviation of this array gives the Dark Signal Non-Uniformity (DSNU).

Fig. 6 shows the results of this dark current measurement. One can see the dark current variations with respect to the temperature of the detector. The dark map at -40°C gives an average dark current of 0.0042 ADU/s and a DSNU of 0.0133 ADU/s (including RON). After conversion with the gain obtained in subsection C, the average dark current is 0.0096 e⁻/s and the DSNU is 0.0303 e⁻/s. These very low values justify *a posteriori* the very long exposures required for that kind of characterisation (up to 16 minutes).
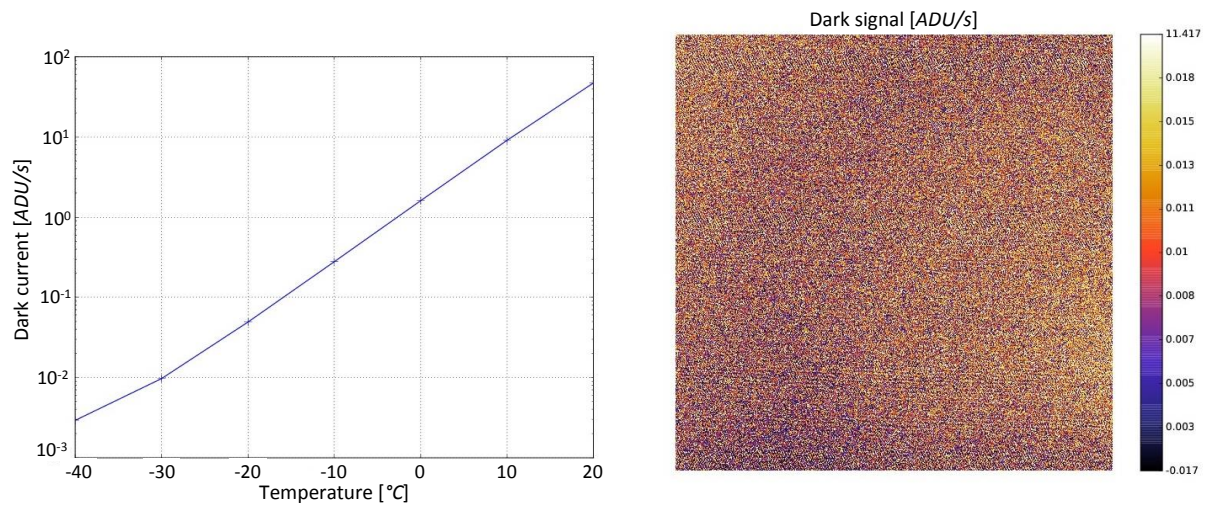

Fig. 6. (*Left*) Dark current vs. temperature. (*Right*) Dark image at -40°C. The colorbar scale is non-linear due to the use of a histogram equalization to enhance small variations on the image.

C. System gain

The system gain is calculated from images taken with different exposure times (from zero to saturation level) using the photon transfer curve (PTC). The slope at the point (0,0) of second order best fit (least squares method) to the variance versus mean curve gives the overall system gain (Fig. 7). This can be explained assuming the Poisson statistics (1).

$$\Delta\, Variance[Electrons^2] = \Delta\, Mean[Electrons] \tag{1}$$

Therefore, the slope is directly equal to the system gain G_S in ADU/e⁻ as shown below (2).

$$\frac{\Delta\, Variance[ADU^2]}{\Delta\, Mean[ADU]} = \frac{G_S^{\,2}}{G_S}\frac{\Delta\, Variance[Electrons^2]}{\Delta\, Mean[Electrons]} = G_S[ADU/e^-] \tag{2}$$

In a first phase, the system gain is determined at the nominal temperature and nominal bias voltages. Then, variations of the gain are also measured by varying the temperature and the bias voltages.

In practice, to get rid of any structure on the CCD, the images with same exposure times are grouped by two. The mean value is calculated over the two images simultaneously and the variance is equal to half the variance of the difference of the two images. Fig. 7 represents the measurement points with the best fit curve (red) from which the gain is estimated. One gets a nominal system gain of 0.4390 ± 0.0005 ADU/e⁻, which corresponds to an amplifier responsivity of 3.66 µV/e⁻ (our electronic chain gain is 0.12 ADU/µV).
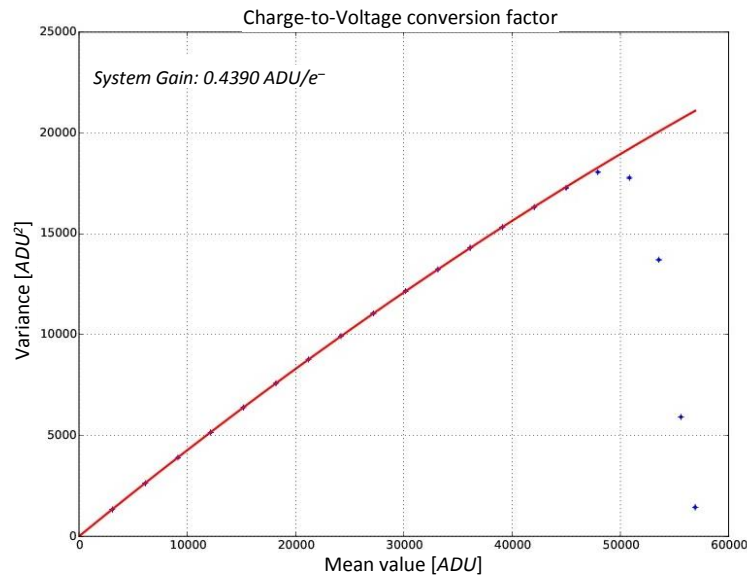
Fig. 7. Variance vs. Mean curve for the CCD gain calculation.

Fig. 8 shows an example of gain measurements made in nominal conditions except for two bias voltages: the Output Drain Level (VOD) and the Reset Drain Level (VRD). Gain variations can then be plotted against the varying parameters, from which we can derive the gain sensitivity in ppm/mV (right part of Fig. 8). This information will be used during the mission to retrieve the exact system gain from the spacecraft electronic data.
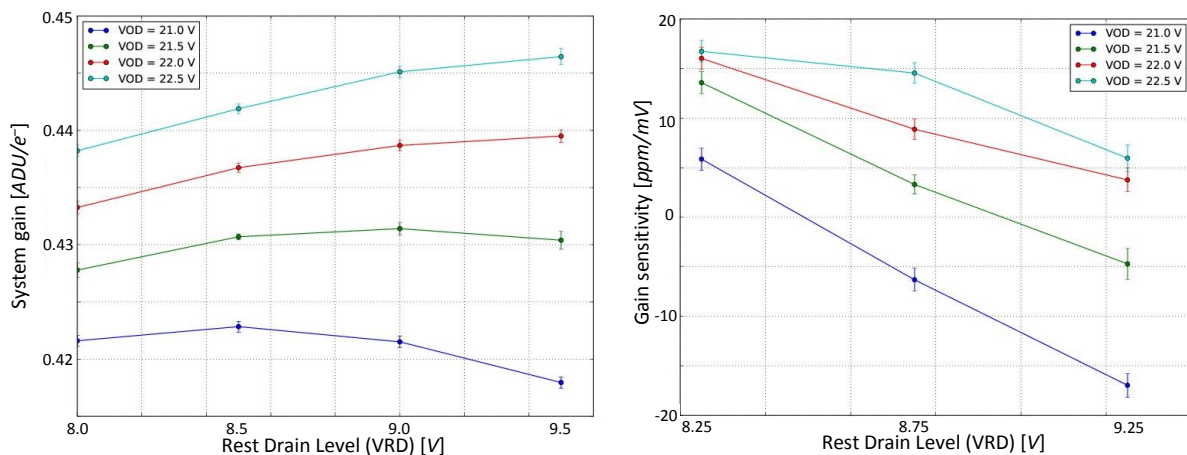

Fig. 8. (*Left*) Variations of the system gain with the VRD bias voltage for different VOD bias voltages.
(*Right*) Sensitivity of the system gain with the VRD bias voltage for different VOD bias voltages.

D. Non-linearity and Saturation level

For the non-linearity and saturation level measurements, the data set taken for the system gain measurement is reused. For both parameters, the mean versus exposure time curve is plotted and the straight-line best fit of the linear part is calculated (Fig. 9). The saturation level is the mean value of the image when the response becomes more than 3% non-linear.

The non-linearity curve corresponds to the relative difference between the best-fit curve value and the measurement. Therefore, small variations at low ADU level will induce higher non-linearity than if same variations occur at higher signal level. Then, the maximum deviation from the best-fit curve on the range 10-to-70% of the saturation level is the non-linearity parameter. The non-linearity parameter is determined at different temperatures and bias voltages around nominal conditions.

Fig. 9 shows the mean signal versus exposure time for the selected CCD. The red straight line is the best linear fit The saturation level, highlighted with the dotted lines (3% of non-linearity), is 55809 ADU or 127.1 ke⁻. The non-linearity variation in the range 10%-70% is represented on the right part of Fig. 9, with a maximum deviation of 0.145%.
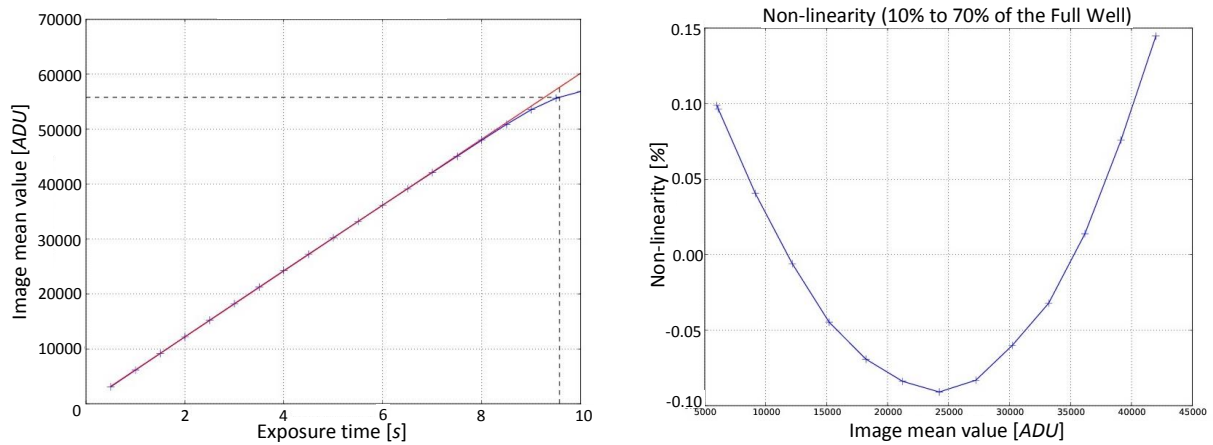
Fig. 9. (*Left*) Mean signal vs. exposure time curve with the straight line best fit (red) and the saturation level highlighted with the dotted lines. (*Right*) Non-linearity curve in nominal conditions.

An example of non-linearity curves for different bias voltages is represented on Fig. 10. On this graph, 16 curves are plotted covering the parameter space of both the VOD and VRD bias voltages, and highlighting the non-linearity variations with the bias voltages.
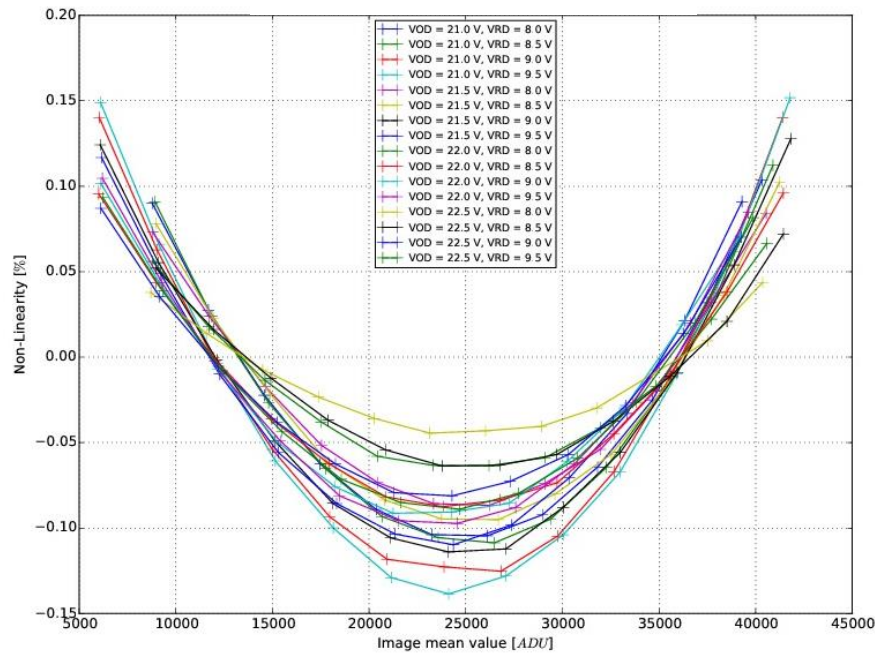

Fig. 10. Non-linearity curves for different conditions in VOD and VRD bias voltages.

E. Photo-response non-uniformity and Flat fields

The purpose of this measurement is to determine the relative sensitivity of each pixel of the CCD. This test is repeated at different wavelengths. As with the other tests, the detector is uniformly illuminated. High signal-to-noise ratio (SNR) images are taken. These images directly define how each pixel responds to a uniform illumination.

The exposure time is set to have an average image signal of about 50% of the full well capacity in order to be in the linear part of the CCD responsivity. The exposure time is constant for a given wavelength, but may vary from a wavelength to another to account for source spectral distribution, system transmission and more importantly detector spectral response (see subsection F). For each wavelength, an average image is computed and then normalised to produce the flat field map. These maps will be used throughout the mission to correct the raw data collected by CHEOPS. Pixels that are below 80% of the average pixel response are considered as defects. Fig. 11 shows an overview of the different flat fields of the CCD at different wavelengths from 400nm to 1100nm.
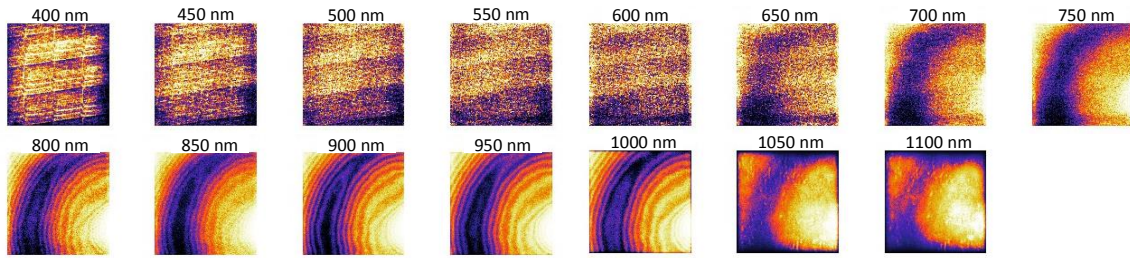
Fig. 11. Overview of the CCD flat fields at wavelengths between 400-1100 nm. The scale is not linear (histogram equalization) and is different for each image. The amplitude of the flat field structures is less than 3% for wavelengths below 700 nm, and increases up to 10% at 1100 nm.

The global PRNU is calculated as the standard deviation of the flat field divided by the mean value. It gives information on the amount of structure in the flat field over the whole sensor.

We define here a *local PRNU* to allow us to have a measurement of the amount of structure in the flat field at different spatial scales. To that purpose, the image is subdivided into small areas in which the PRNUs are calculated. We define the average of these values as the local PRNU. We see on Fig. 12 that the local PRNU, especially at a scale of 3x3 to 5x5 pixels, is substantially smaller than the global PRNU. This tells us that the effect of the satellite pointing wobble, which is precisely in the 3-5 pixels rms range, will be significantly lower than what could be anticipated from the global PRNU alone[1].

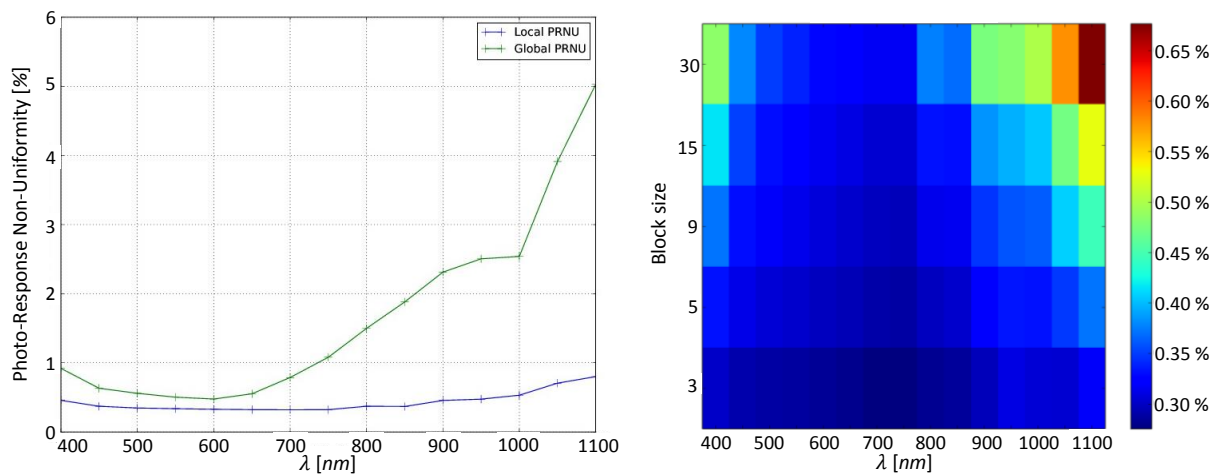Fig. 12 illustrates the different PRNU results obtained on the CCD.

Fig. 12. (*Left*) Global and 30x30-pixel local PRNU variations with respect to the wavelength. (*Right*) Local PRNUs with respect to the illumination wavelength and the block size (a block size of 5 means 5x5-pixel areas).

F. Quantum efficiency

The quantum efficiency (QE) of the CCD is calculated according to the following equation (3), which corresponds to the ratio of electrons generated in the CCD to the number of incoming photons.

$$QE_\% = \frac{S_0 \cdot h \cdot c}{G_s \cdot t_i \cdot P_w \cdot A \cdot \lambda} \times 100$$

(3)

where S_0 is the CCD output signal [ADU]
           h is Plank's constant [J.s]
           c is the speed of light [m/s]
           G_S is the overall system gain [ADU/e⁻]
           T_i is the integration time [s]
           P_w is the incident light power [W/m²]
           A is the pixel area [m²]
           λ is the illuminating wavelength [m]

---

[1] We make the hypothesis that the flat field measurement error is proportional to the amplitude of the flat field.

The incident spectral power is measured with a calibrated photodiode fed with a fibre pick-up in the integrating sphere. The wavelength-dependent responses of the diode and the fibre are taken into account for the calculation of the QE. However, the ratio of the amount of light reaching the diode to the one reaching the CCD has not been measured. Therefore, the absolute values of the quantum efficiency are not correct but their relative variations are. Fig. 13 shows the normalized quantum efficiency, called relative QE, measured for the flight CCD. The estimated precision of each data point is represented by the error bar on the graph.
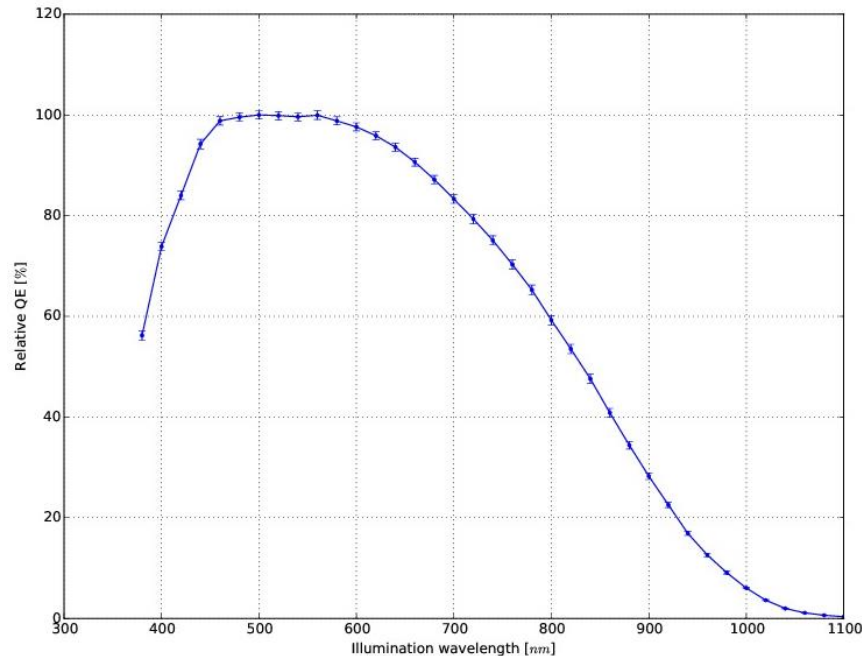

Fig. 13. Relative quantum efficiency.

IV. CONCLUSION:

We have measured the performances of three flight model CCDs on our test bench to a precision that is commensurate to the CHEOPS requirements. These measurements have led to the selection of the best detector for the mission.

In the near future, this CCD will be integrated to the payload and tested as a complete system. This calibration will be performed in the CHEOPS integration facilities for which a specific on-ground calibration bench has been developed [3,4].

REFERENCES

[1]   W. Benz et al, "CHEOPS: Scientific Objectives, Mission Concept, and Challenges for the Scientific Community", the 4S Symposium 2014.
[2]   V. Cessa et al, "CHEOPS: A space telescope for ultra-high precision photometry of exoplanet transits", International Conference on Space Optics 2014.
[3]   F.P. Wildi, B. Chazelas, A. Deline, M. Sordet, and M. Sarajlic, "The CHEOPS' instrument On-Ground calibration system", *Proc. SPIE 9605, Techniques and Instrumentation for Detection of Exoplanets VII*, 96051B, September 2015.
[4]   F.P. Wildi, B. Chazelas, A. Deline, M. Sarajlic, and M. Sordet, "The CHEOPS' calibration bench", International Conference on Space Optics 2016.
[5]   "EQ-99XFC LDLS™" from Energetiq Technology, Inc., 2014. URL: http://www.energetiq.com/DataSheets/EQ99XFC-Data-Sheet.pdf
[6]   F.P. Wildi, A. Deline and B. Chazelas, "A white super-stable source for the metrology of astronomical photometers", *Proc. SPIE 9605, Techniques and Instrumentation for Detection of Exoplanets VII*, 96051T, September 2015.